



Thin-wall micromachining of Ti–6Al–4V using micro-wire electrical discharge machining process

Mahavir Singh¹ · Amandeep Singh¹ · J. Ramkumar¹

Received: 23 December 2018 / Accepted: 15 July 2019 / Published online: 26 July 2019
© The Brazilian Society of Mechanical Sciences and Engineering 2019

Abstract

Machining of delicate thin members having extremely small thickness as compared to the other two dimensions is a precarious task when performed using conventional fabrication techniques. Non-contact machining process, such as micro-wire electrical discharge machining (micro-WEDM) process, an advanced means of machining, offers an appropriate way to machine thin-wall structures in an utmost precise manner. In the present work, thin-wall micromachining of Ti–6Al–4V is performed while utilizing the contactless, negligible thermal damage, and deformation-free nature of micro-WEDM process energized through the resistance–capacitance generator. The objective is to explore the feasibility of a minimum possible wall thickness. Performing the thin-wall micromachining using wire step-over approach, it is established that a wall of average thickness 8.47 μm with an end deflection and a wall of thickness about 15 μm free from end deflection is possible to fabricate using micro-WEDM process. It achieves a high aspect ratio of 70 corresponding to the minimum thickness of the wall. What's more, a theoretical analysis is carried out to illustrate the functional relationship between wall-end deflection with workpieces' thermophysical properties, discharge parameters, and the geometric parameters of the wall. Finally, the comparative assessment of wall-end deflection and volumetric material removal rate attained with three different materials, namely Ti–6Al–4V, mild steel, and SS-304, reveal that thermophysical properties of workpiece material play a critical role in determining the wall-end deflection and the resultant volumetric material removal rate.

Keywords Thin wall · Wall deflection · Wall thickness · Discharge energy · Step-over · MEMS

1 Introduction

Thin-wall micromachining is conceived as a domain of micro-fabrication wherein the machining of thin wafers of various materials, as well as the components with an extremely small thickness, is created. Generally, structures having aspect ratio (height to thickness ratio) somewhat greater than five are categorized as thin walls [1]. It has gained significant importance in last few decades with the prolific developments in microelectromechanical system (MEMS). Though the majority of the MEMS devices are focused on materials such as silicon and polymers, the metals such as titanium and its alloys are appealing to the

researchers. Titanium alloys possess unique physical and mechanical properties such as low density, high corrosion resistance, stability during testing of microbeams with exceptional biocompatibility [2]. Broadly, the thin-wall machining can be classified into two categories. The first category includes the slicing of thin wafers of materials such as silicon, germanium, etc., for solar cell application. Thin wafers slicing contemplates thinning of wafers as well as the enlargement of the cross-sectional area of the wafer. Whereas, in the second category, thin-wall machining is usually performed with the objective of minimization of wall thickness with a small cross-sectional area as compared to thin wafers.

The productivity while machining thin wafers is largely determined by the minimum kerf-loss and reduced thickness of the wafer. Moreover, minimization of wafer thickness realizes higher conversion efficiency to cater need of the hour of solar cells requiring conversion efficiency higher than 23–25% [3]. The manufacturing methods for the creation of thin-wall structures are in an emerging stage

Technical Editor: Lincoln Cardoso Brandao.

✉ Mahavir Singh
mahavir@iitk.ac.in

¹ Department of Mechanical Engineering, Indian Institute of Technology Kanpur, Kanpur 208016, India

as none of the available techniques has the requisite capabilities to fabricate these structures impeccably. Several traditional as well as non-traditional methods for the slicing or fabrication of thin slices are incorporated by various researchers. These methods include the wire saw method, internal diameter sawing, plasma etching, electroplating, additive manufacturing, WEDM process, etc. [4]. Multi-wire saw method has demonstrated higher throughput and low kerf-loss as compared to the aforesaid techniques [5]. Laser cladding has also been attempted to fabricate a thin wall of thickness 400 μm [6]. These methods are capable of producing thin wafers with a higher rate of productivity, but the required dimensional accuracy, surface finish, damage free components, etc., cannot be achieved with a high degree of success. Some of the techniques are limited by mechanical forces and vibration associated with them due to severe tool workpiece contact; others are limited by the deflection of the tool itself. Additive manufactured parts lack the required strength in the build direction besides the poor surface finish of the manufactured parts. Plasma and laser welding/cladding are the thermal processes wherein the heat load restricts the minimum thickness that can be achieved. Micro-WEDM, an advanced machining process, owing to its non-contact nature and requisite potential to reduce the discharge energy and discharge duration has found wide applicability in machining of thin wall/thin wafers with superior dimensional accuracy and negligible damage. In the present research, the objective is to machine Ti-6Al-4V workpiece in order to obtain the thin walls with minimum possible wall thickness. The micro-WEDM process had been used for the slicing of silicon ingots to produce thin silicon and germanium wafers for PV fuel cell applications [7, 8]. It had shown a promising inclination in minimizing the wafer thickness to 130–150 μm with uniformity of thickness along the length [7]. The efforts to minimize the wafer thickness and enhance the slicing rate are some of the critical issues in the thin-wall machining. The micro-WEDM process has extensively been used for the slicing of thin silicon wafers owing to its contactless nature. Wafers from *n*-Type single-crystal silicon ingot and precise cutting of polished single-crystal silicon using different dielectrics and applying the suitable mask on both sides of the wafer were performed using WEDM process [9–11]. The thermal damage caused to the wafer was observed to be minimum using various characterization methods such as SEM, TEM, and Raman spectroscopy [12]. A thin layer of thermal damage was observed on the wafer surface, and it was largely influenced by the exposure duration of plasma. The influence of controlled input parameters on the resultant thickness of the wafers and kerf-loss were analysed exclusively [13]. Researchers have also tried to propose a hybrid technique for wafer slicing which combines wire saw method and WEDM together. The hybrid technique showed an improvement in slicing

efficiency, reduced the scratches on the wafer, and lowered the kerf-loss [14]. The slicing operation consists of both mechanical slicing and spark erosion and hence produces higher efficiency. An effort was also made to perform thin-wall micromachining of Ti-6Al-4V. The objective to reduce the wall thickness using the WEDM process had resulted in the formation of a thin wall of 61 μm thickness [15]. The transistor-based power generator employed for the WEDM processing of thin wafer lacks the required minimum thickness of the wafers. The decisive drawbacks of the transistor-based circuit include higher discharge energy, large bubble collapsing force, inability to use ultra-thin wire tool, severe wire vibration due to higher exploding pressure of plasma channel as well as high heat load applied. These inadequacies have often restricted the fabrication of thin wafers not below 100 μm thickness. Besides discharge parameters, the yield strength and thermal conductivity of the material were considered as the deciding factors in the dimensional stability of the thin wall [16]. Low thermal conductivity and yield strength of the work material prevent the effective removal of heat and deform the wall under plastic deformation, respectively. Thermo-physical modelling of WEDM for thin wall component had predicted temperature distribution in the wall, and thus, deformation characteristics and residual stresses were evaluated [17]. Experimental validation of residual stresses at different input conditions was carried out. Resistance-capacitance (RC)-based power generator especially used in micro-WEDM machines has the capability to reduce the discharge energy per pulse and pulse-on time by substantially reducing the capacitance of the capacitor. Thus, nanopulses with extremely small discharge energy per pulse are possible to attain using RC-based power generator. Reduced discharge energy per pulse would facilitate the low thermal damage to the wall as the duration for which energy is applied also lowered down subsequently. Owing to the above-mentioned merits, RC-based micro-WEDM process is chosen to realize the thin walls in the current work. The literature review does not reflect an extensive study pertaining to thin wall machining. Conventional techniques of fabrication are inappropriate to manufacture extremely thin structures. Using WEDM process, the minimum wall thickness achieved with Ti-6Al-4V is not below 60 μm in the literature. This work presents a possibility of fabricating ultra-thin wall, as low as 8–10 μm thin, using micro-WEDM process. Moreover, a theoretical understanding is required to illustrate the relationship between wall-end deflection with influencing parameters such as discharge parameters, geometric parameters of the wall and thermophysical properties of the workpiece material. This gap is being narrowed in the present research work.

The potential applications of thin-wall machining consist of various microsensors and actuators used in MEMS devices. One of the predominant applications of these

thin-wall structures is in microsensors where a finite deflection of a microcantilever beam determines the presence of various microorganisms and bacteria. It also acts as physical, chemical, and biological sensors [18]. Various other applications include actuators, sensors, viz. switches, capacitive pressure sensors, accelerometers, filters, resonators, etc. [19]. The thin wall of Ti-6Al-4V due to its excellent biocompatibility has been used as a dental reinstatement [20]. MEMS parallel plate actuator with two microbeams one having cantilever configuration and other fixed, separated by a small distance, is another area of application of thin-wall machining of conductive materials. The cantilever beam is actuated with a positive potential, and under the redistribution of charges, the cantilever beam deforms and is attracted towards the fixed beam which is at a negative potential. Either the continuous deformation of cantilever beam results in an equilibrium state at which the further deformation ceases or it can attain a pull-in stage where both the beams contact physically [21]. Micro-thin cantilever specimens are also used in the study of time-dependent behaviour of materials such as creep [22]. The multi-slit thin-wall array can be used as a tool electrode in ECM process as there is no tool wear in the process. The wear-free nature of tool in ECM process makes it viable to use these delicate tools, which otherwise deforms severely.

In the current work, the endeavour is to minimize the thickness of the thin wall by utilizing the advantages of substantially reduced discharge energy and small discharge duration associated with an RC-based power generator. Wire displacement/step-over approach, in which the wire tool is displaced with an amount equal to the kerf-loss generated at the certain combination of discharge energy and feed rate, in addition to the predicted thickness of the wall, is used for thin-wall machining. Further, an effort has also been made to determine the wall-end deflection in terms of different parameters

involved in the process. Finally, a comparative assessment is performed to show the deflection behaviour and material removal rate attained with three different workpiece materials.

2 Experimental setup and methodology

2.1 Experimental setup

Multipurpose integrated micro-machine tool: DT-110 (Mikrottools Pte. Ltd., Singapore) is used to conduct the micro-WEDM experiments for thin-wall machining. Figure 1 represents the micro-WEDM setup in the DT-110 machine tool and the nomenclature of the different elements in the attachment. The machine tool is furnished with an RC-based power generator that has the flexibility of varying the capacitance of the capacitor and open circuit voltage with a constant charging resistance of 1 K- Ω . A tungsten wire of diameter 70 μm is used as a tool electrode. The wire is moved continuously between the wire supplying and wire collecting wheels. A series of wire guide cum tensioner ensures the proper running and adequate tension to the wire. Titanium grade-5 alloy (Ti-6Al-4V) with a uniform thickness of 800 μm is selected as the workpiece material. An initial inter-electrode gap of 20 μm , wire tension of 10%, and a threshold value of 20 are kept constant for all the treatments.

2.2 Kerf-loss in thin-wall micromachining

There are two important aspects while conducting thin-wall machining: the resultant minimum thickness of the wall and the kerf-loss generated for achieving the required wall thickness. Kerf-loss is the width of the feature generated due to machining through wire electrode. It consists of wire

Fig. 1 Micro-WEDM attachment in the DT-110 machine tool

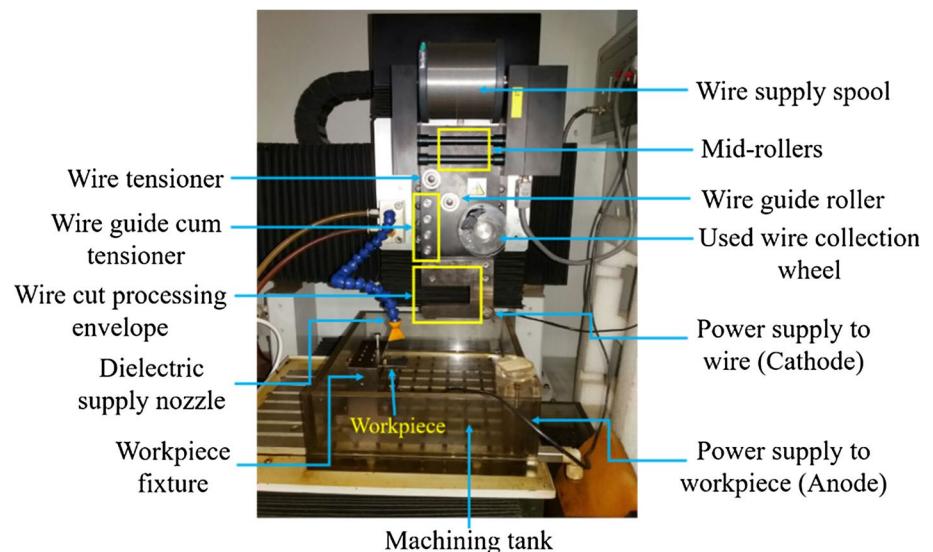
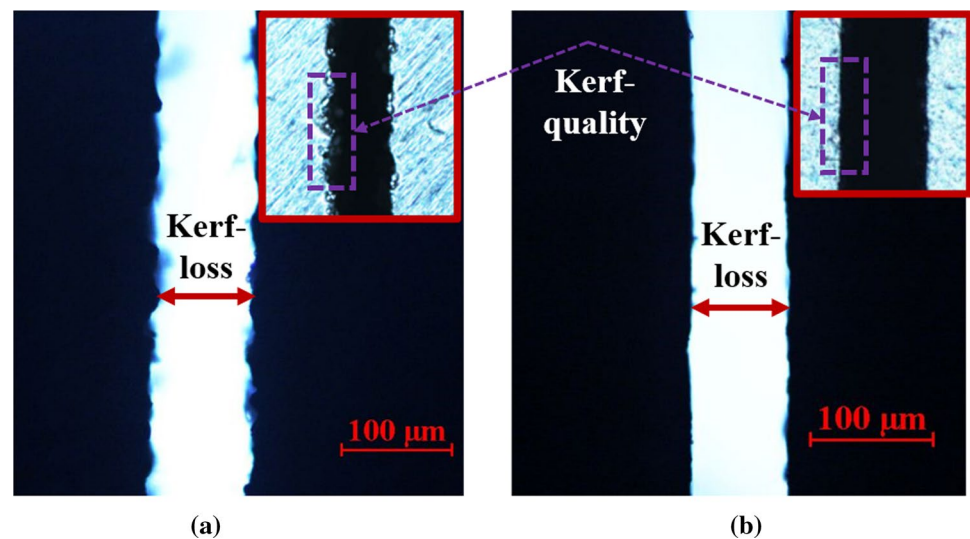


Fig. 2 Kerf quality representation using optical microscopic images of micro-slit machined at **a** 2880 μJ discharge energy, **b** 0.72 μJ discharge energy (at feed rate: 6 $\mu\text{m}/\text{s}$ and wire speed: 10%). (Adapted from [24])



diameter plus two times the radial overcut between the wire and the workpiece. It is known that an increase in kerf-loss results in a decrease in the wall thickness. This phenomenon eventually leads to the reduction in wall thickness to a magnitude at which the wall is unable to withstand the thermal load, wire vibration, and bubble collapsing forces induced during the operation. Therefore, it is inevitable to conduct the kerf-loss determination prior to thin-wall machining. Exploratory experiments are performed using One Factor At a Time (OFAT) approach by varying discharge energy and wire feed rate. The discharge energy in the micro-EDM/WEDM process is a combination of open circuit voltage (V) and capacitance of the capacitor (C) which is represented as follows [23].

$$E = \frac{1}{2} \times C \times V^2$$

The discharge energy was varied at four distinct levels (0.72 μJ , 72 μJ , 720 μJ , and 2280 μJ) by varying the capacitance while keeping open circuit voltage constant at 120 V. The open circuit voltage has less significant effect on discharge energy as the breakdown voltage invariably remains constant for fixed combination of inter-electrode gap and dielectric, and thus kept constant. The wire feed rate was varied at three levels (2 $\mu\text{m}/\text{s}$, 4 $\mu\text{m}/\text{s}$, and 6 $\mu\text{m}/\text{s}$) considering the short circuits that occur at higher feed rate. The output responses of interest were average cutting rate and average kerf-loss. The average cutting rate depicts the economic viability of a process as it determines the length of cut per unit time, whereas the average kerf-loss determines the dimensional accuracy of any cutting process. The average kerf-loss achieved at different levels of discharge energy and wire feed rate are summarized as follows.

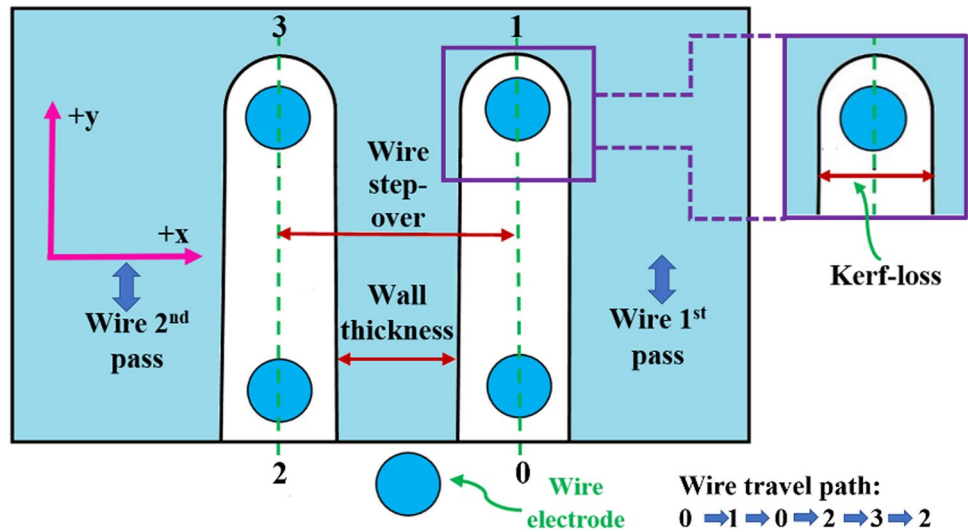
The average kerf-loss at 2880 μJ discharge energy, with all levels of wire feed rate, is found to be around 100 μm .

Moreover, the quality of kerf in terms of edge quality and uniformity of the cut show an unsatisfactory result, and it is generally recommended to use this energy level for rough cutting operation where kerf quality is not a prime interest. Further, at 720 μJ and 0.72 μJ , the average kerf-loss remains almost constant, and it is approximately equal to $80 \pm 4 \mu\text{m}$. At 0.72 μJ discharge energy, though the energy per-pulse is low as compared to that at 720 μJ , the higher frequency of sparks invalidates the reduction in the volume of material removal per pulse. Therefore, the required decrease in kerf-loss at 0.72 μJ is not obtained, and it is almost equal to that obtained at 720 μJ . At 72 μJ discharge energy, the average kerf-loss lies in between that obtained at the highest and lowest discharge energy, with an approximate value of $85 \pm 2 \mu\text{m}$. The slit machined at 2880 μJ and 0.72 μJ discharge energies is shown in Fig. 2a, b, respectively. The investigations pertaining to the accurate explanation of the variation of kerf-loss and average cutting rate with different input parameters are not reported in this work. The focus of this study is on determining the appropriate wire displacement/step-over essential for the precise evaluation of intended wall thickness. The wire displacement/step-over required for generating a wall of certain thickness includes the average kerf-loss in addition to the thickness of the wall. It is established during the study that the wire must be displaced from its previous path to the next path by a distance of 90 μm to generate a thin wall of the thickness of the order of 10 μm , at discharge energies of 0.72 μJ and 720 μJ .

2.3 Thin-wall micromachining: methodology

Figure 3 illustrates the methodology implemented for the parallel multi-slit thin-wall micromachining. The prior information of kerf-loss at a fixed combination of discharge energy and wire feed rate enables the determination of wire

Fig. 3 Schematic representation of multi-slit thin-wall micromachining showing the path travelled by the wire



step-over from the current pass to the next parallel pass. In the first pass, wire performs cutting operation in 0–1 direction up to the desired length and returns from 1 to 0 to the original position in rapid traverse mode (no cutting operation). Then the wire is displaced by an amount known as wire step-over from 0 to 2. The second pass of wire follows the similar path, 2–3 and 3–2, as followed in the first pass to generate a wall in between the two passes. The procedure is repeated until the last wall is machined. It can be noted that the number of passes is always one more than the number of walls generated.

OFAT experimental method is used to conduct the experiments to determine the minimum wire step-over at which a wall of finite thickness can be generated. The inadequate wire step-over between two passes of wire travel results in

overlapping of kerf-loss and produces no wall as shown in Fig. 4a wherein the wire step-over is 80 μm. Moreover, wire step-over below 90 μm produces a wall which is unstable and eventually deforms. Therefore, the minimum step-over is selected as 90 μm. However, a wire step-over above 110 μm increases the wall thickness which is contrary to the interest of the current work. Hence, wire step-over is selected between 90 and 110 μm in the steps of 10 μm. SEM image of a deflection free wall fabricated at a wire step-over of 100 μm is shown in Fig. 4b.

OFAT experiments reveal a less significant effect of both wire feed rate and wire tension on the wall-end deflection. However, wire feed rate influences the average cutting rate and kerf-loss. Therefore, the maximum feed rate of 6 μm/s is selected for thin wall machining keeping in view the frequent

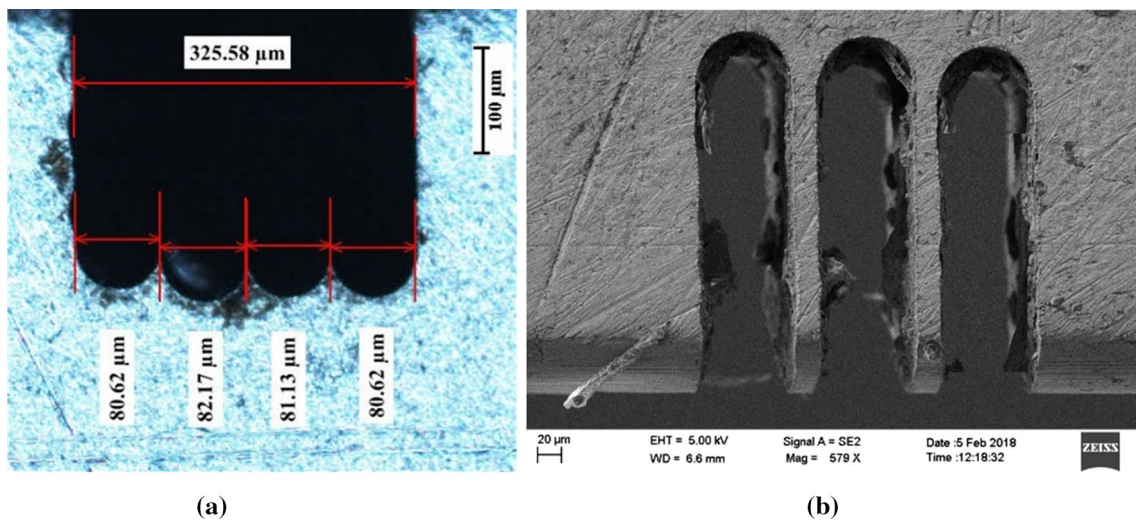


Fig. 4 a Inadequate wire step-over of 80 μm produces no wall, b SEM image of the stable wall machined at 100 μm wire step-over (at discharge energy: 720 μJ and feed rate: 6 μm/s)

short circuit occurrence at feed rate above 6 $\mu\text{m/s}$. The wire used in the present work is highly susceptible to breaking as the combined effect of the thermal energy of discharge and wire tension reduces its tensile strength. Therefore, wire tension is kept constant at 10%.

3 Results and discussion

3.1 Experimental results of thin wall machined at different discharge energy conditions

The thin-wall micromachining operation is performed using 70 μm tungsten wire on the Ti–6Al–4V workpiece (800 μm thickness) at three different levels of discharge energy (720 μJ , 72 μJ , 0.72 μJ) keeping wire feed rate constant at 6 $\mu\text{m/s}$. Three sets of wire step-over, 90 μm , 100 μm , and 110 μm are selected to generate the thin walls of varying thickness as per the step-over. Table 1 shows the minimum average wall thickness at a certain combination of wire displacement and discharge energy. The minimum average wall thickness of 8.47 μm is achieved at 0.72 μJ discharge energy and 90 μm wire displacement. The thickness of the wall is measured at three different locations (start, mid, and end of the slit), and the average value is reported in Table 1. At 90 μm wire displacement and 72 μJ discharge energy, it is observed that the wall deformed severely and vanished from its original position probably due to a very small thickness that could not withstand the thermal load and wire vibration.

The analysis of average kerf-loss carried out in Sect. 2.2 is useful in determining the requisite wire displacement/step-over from previous to the next parallel pass. It is already reported that the kerf-loss at 0.72 μJ and 720 μJ discharge energies, and wire feed rate of 6 $\mu\text{m/s}$, is approximately 80 ± 4 μm . The kerf-loss varies over a range depending upon the flushing conditions, wire feed rate, and discharge energy. Therefore, obtaining a wall of thickness about 10 μm requires a wire to be displaced by 90 μm . This is experimentally verified by the average wall thickness obtained at the above-mentioned conditions. Figure 5a, c represents these wall thicknesses at 720 μJ and 0.72 μJ discharge energies, respectively. However, the average kerf-loss at 72 μJ

discharge energy is quite high (approximately 85 ± 2 μm), and the corresponding wall thickness obtained with 90 μm wire step-over would have been about 4–5 μm . This thickness is very small to sustain the thermal load due to discharge energy, hydrodynamic pressure of the dielectric fluid, and mechanical forces due to wire vibration. The resultant effect of these factors is the severe deformation of the wall which eventually results in no wall generation at 72 μJ discharge energy and 90 μm wire displacement. It is seen in Fig. 5b (that shows the wall thicknesses at 72 μJ discharge energy) that the first wall is completely disappearing from its original position. A minimum wall thickness of 8.31 μm and an average wall thickness of 8.47 μm are accomplished at 0.72 μJ discharge energy and 90 μm displacement (Fig. 5c). The aspect ratio (ratio of the wall length and its thickness) is around 70 at the minimum thickness of the wall. However, the wall is deflected at the end, due to the small thickness that deforms it plastically under the thermal load. It has also been observed that a wall of average thickness about 15 μm or above is stable and does not undergo significant deflection.

The average wall thickness increases almost linearly with an increase in wire displacement as the more unmachined material is available between two parallel passes of wire. Figure 6 represents the variation of wall thickness with wire displacements at 720 μJ discharge energy. Yet, reducing the wire displacement below 90 μm resulted in extremely small wall thickness and it deformed severely. A similar trend is observed at other two discharge energies.

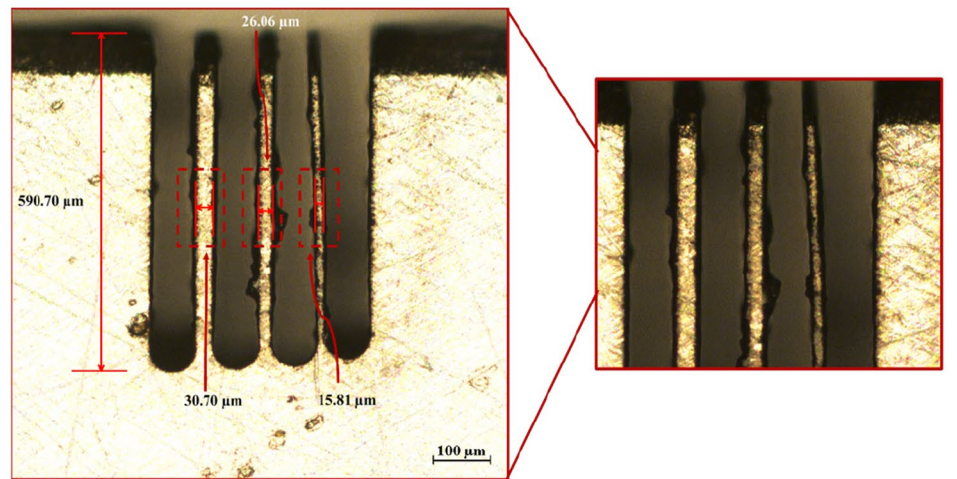
The minimum achievable wall thickness at three distinctive energy levels is shown in Fig. 7. The figure illustrates that the minimum thickness of the wall is achieved at 0.72 μJ discharge energy. However, at 720 μJ discharge energy, the minimum wall thickness is about 16 μm . At 72 μJ discharge energy due to high kerf-loss, it is not possible to achieve any wall at a wire displacement of 90 μm . Again, increasing the wire displacement to 100 μm a wall of average thickness about 18 μm is possible to machine. Therefore, the minimum wall thickness at 72 μJ discharge energy reported in Fig. 7 is the value obtained at 100 μm wire step-over. A logarithmic scale has been used for discharge energy to represent the graphical plot best.

Wall generation rate refers to the ratio of total wire travel for the fabrication of a single wall to the total time required for the travel. It is clearly understood that a single wall requires two wire passes on either side of it. Therefore, the generation rate considers the total length of the slit for two passes and time of machining. The wall generation rate is found to be nearly the same at 0.72 μJ and 720 μJ discharge energies (Fig. 8). The constant feed rate, 6 $\mu\text{m/s}$, used at both the energy levels shown to be inadequate to quickly compensate the frontal spark gap which enlarges due to the formation of larger size crater at 720 μJ discharge energy.

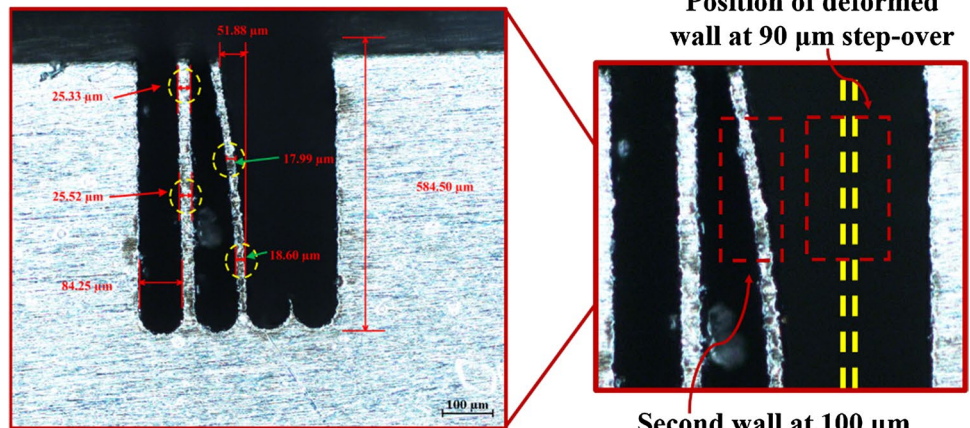
Table 1 Minimum average wall thickness at various combinations of wire displacements and discharge energy

S. No.	Wire displacement (μm)	Average wall thickness (μm) at different discharge energies		
		720 μJ	72 μJ	0.72 μJ
1.	90	16.4	No wall	8.47
2.	100	24.17	18.2	20.15
3.	110	32.09	25.4	31.65

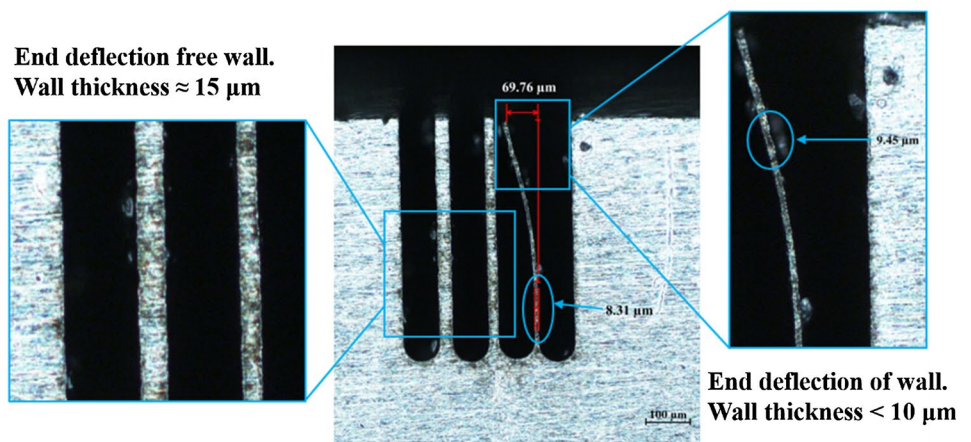
Fig. 5 Multi-slit thin-wall machining and wall thicknesses **a** at discharge energy: 720 μJ , **b** at discharge energy: 72 μJ , and **c** at discharge energy: 0.72 μJ (with wire displacements of 90 μm , 100 μm , and 110 μm from right to left, and constant feed rate of 6 $\mu\text{m/s}$)



(a)



(b)



(c)

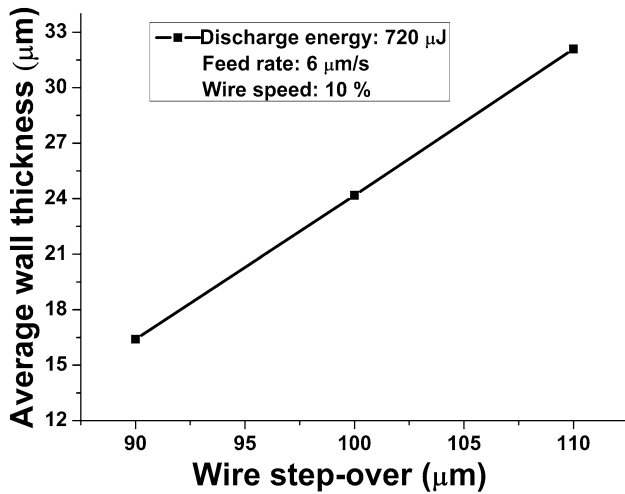


Fig. 6 Variation of average wall thickness with wire step-over

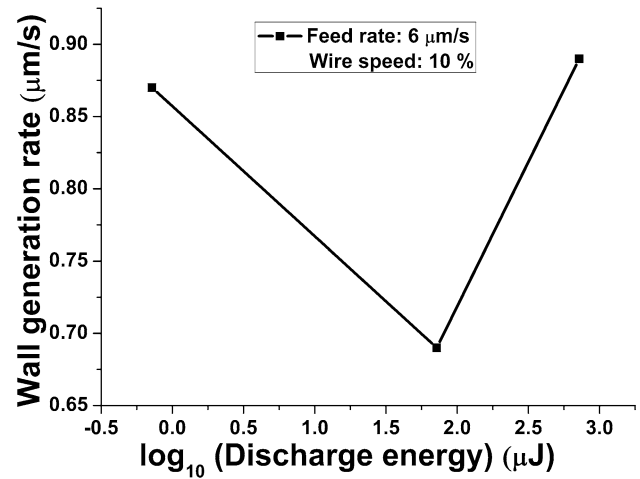


Fig. 8 Variation of average wall generation rate with discharge energy at wire step-over of 90 μm

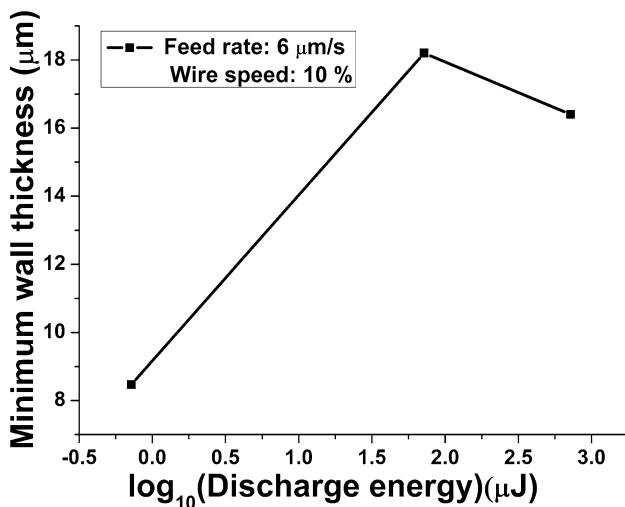


Fig. 7 Variation of minimum average wall thickness with discharge energy at wire step-over of 90 μm

Consequently, the required improvement in wall generation rate is not achieved at this discharge energy. However, at 72 μJ discharge energy, the wall generation rate is considerably low, and the average kerf-loss is very high. The frequency of sparks and discharge energy is such that the time necessary for the removal of debris is inadequate. The inability of the wire to move continuously forward due to poor flushing of molten liquid and debris result in the poor rate of wall generation, which in turn increases the time available for secondary sparks. Therefore, the wall generation rate decreases. The higher time of secondary sparks due to continuous retracting of wire caused by poor debris flushing results in larger kerf-loss at 72 μJ discharge energy.

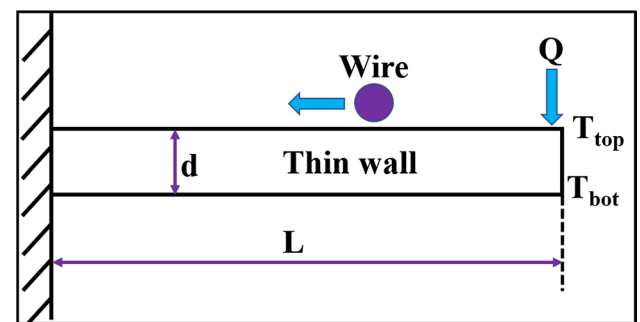


Fig. 9 Schematic diagram illustrating a thin wall subjected to a single spark at the free end

3.2 Wall-end deflection in micro-WEDM process

In this section, an attempt is made to show the functional relationship of wall-end deflection with different influencing parameters such as micro-WEDM input parameters, thermo-physical properties of the workpiece material, and geometric parameters of the wall. To develop the relationship, consider a thin wall having thickness d and length L as shown in Fig. 9. The wall thickness is the thickness of material that is left unmachined between two parallel passes of the wire travel, and it is absolutely different from the thickness of the workpiece. The third dimension of the wall normal to the thickness is significantly high.

Following assumptions have been made in the current relationship development:

- (a) A single spark is assumed to be occurring at the free end of the wall. The wall is considered to be a cantilever beam of a certain length.

- (b) The lateral vibration of the wire is negligible, i.e. there is no mechanical force acting on the wall.
- (c) The dielectric flow pressure is such that it does not contribute to the bending characteristics of the wall.
- (d) The thickness of the wall is significantly small as compared to its length, width, and the diffusion of heat is unidirectional, i.e. across the wall thickness. The thickness of the workpiece sheet is considered to be the width of the wall.
- (e) The machining has been performed at one side of the wall (bottom), and the residual thermal stresses are negligible as the dielectric takes away the heat by convection.
- (f) Only the conduction of the fraction of heat applied to the workpiece is considered. The heat of discharge is conducted from the top to the bottom of the wall.

The thermal energy required for the melting and evaporation of the workpiece is supplied from the plasma channel. The discharge energy of plasma is distributed among dielectric, tool, and workpiece. The fraction of heat incident to the workpiece is conducted in the bulk material due to conduction. According to the thermal conduction of heat across the thin wall of thickness d , the heat transfer rate is given by:

$$Q = \frac{KA(T_{top} - T_{bot})}{d} \tag{1}$$

$$T_{top} - T_{bot} = \frac{Qd}{KA}$$

where K is the thermal conductivity of workpiece material, A is the cross-sectional area of the wall, and d is the wall thickness. T_{top} and T_{bot} are the temperatures at the top and bottom of the wall.

Q is the rate of heat transfer across the wall, and it is given by $Q = \frac{\beta E}{T_{on}}$, such that β and E represent the fraction of discharge energy available to the workpiece and the total discharge energy per spark, respectively. β generally varies with the tool-workpiece combination, type of dielectric fluid, etc. In the present study, β is assumed to be 0.39 [25]. T_{on} is the pulse-on time of a single spark. For an RC-based power generator used in the micro-WEDM machine, the discharge energy and pulse-on time for a single spark/pulse are expressed as follows [26].

$$E = \frac{1}{2} CV^2 \tag{2}$$

$$T_{on} = -0.1RC \ln \frac{(V - V_d)}{V} \tag{3}$$

where R is the charging resistance and C is the capacitance of the capacitor. V is the open circuit voltage, and V_d is the discharge/breakdown voltage which is equal to $\frac{V}{2}$ for maximum energy [27].

Due to temperature variations, the thin wall experiences strain at the top and bottom, respectively. If y is the deflection of the wall at the free end, its curvature due to thermal strains is given by:

$$\frac{d^2y}{dx^2} = \frac{\alpha(T_{top} - T_{bot})}{d} \tag{4}$$

where y is the deflection of the wall normal to its axis, and x is the distance from the fixed end. α is the coefficient of linear expansion of wall material. $\alpha(T_{top} - T_{bot})$ represents the equivalent thermal strains across the wall of thickness d .

The first integration of Eq. (4) gives the slope of the wall at the free end:

$$\frac{dy}{dx} = \theta = \frac{\alpha(T_{top} - T_{bot})}{d}x + M \tag{5}$$

where θ and M are the slope of the wall and constant of integration, respectively.

Further, integrating Eq. (5), we get the following expression for wall deflection:

$$y = \frac{\alpha(T_{top} - T_{bot})}{2d}x^2 + Mx + N \tag{6}$$

M and N are the constants of integration calculated by applying the suitable boundary conditions (BCs). At the fixed end of the wall, the wall deflection and slope are zero.

BCs: At $x = 0, y = \frac{dy}{dx} = 0$. Thus $M = N = 0$

Putting $M = N = 0$ in Eqs. (5) and (6), the slope and deflection of the wall at a distance x from the fixed end are expressed as:

Slope of the wall : $\theta = \frac{\alpha(T_{top} - T_{bot})}{d}x$ (7)

Deflection of the wall : $y = \frac{\alpha(T_{top} - T_{bot})}{2d}x^2$ (8)

Putting $x = L$ in Eqs. (7) and (8), the slope and the deflection at the free end of the wall due to a single spark are calculated as:

Slope of the wall at the free end: $\theta = \frac{\alpha(T_{top} - T_{bot})}{d}L$ (9)

Deflection of the wall at the free end : $\delta = \frac{\alpha(T_{top} - T_{bot})}{2d}L^2$ (10)

Putting $(T_{top} - T_{bot})$ from Eq. (1) into (10), the expression for wall deflection at the free end is established as follows:

$$\delta = \frac{\alpha Q}{2KA}L^2 \tag{11}$$

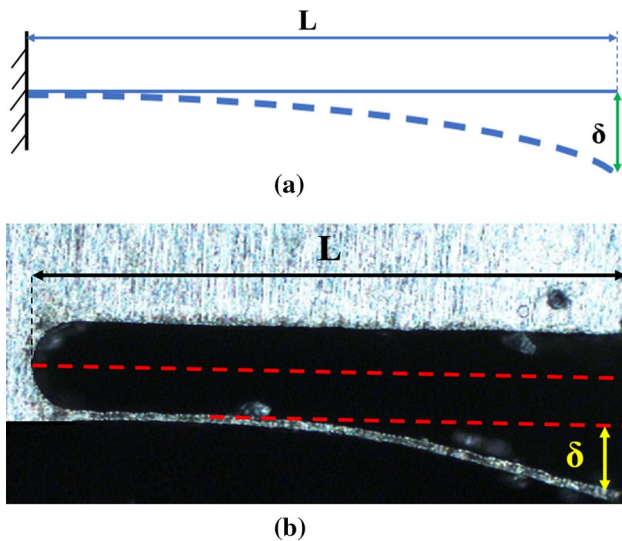


Fig. 10 **a** Schematic illustration of the end deflection of a cantilever beam, **b** the deformed wall shows similarity to the deflection of a cantilever beam

Further putting $Q = \frac{\beta E}{T_{on}}$ in Eq. (11), the final expression for wall-end deflection in terms of discharge energy per pulse is given as follows:

$$\delta = \frac{\alpha \beta E}{2KAT_{on}} L^2 \tag{12}$$

The expression in Eq. (12) represents the end deflection of the wall due to a single spark applied at the free end. It is evident here that the wall deflection at the free end is directly related to the coefficient of thermal expansion (α), discharge energy per pulse (E), and free length of the wall (L). However, the wall deflection is inversely proportional to the thermal conductivity of workpiece material (K), pulse-on time (T_{on}), and cross-sectional area of the wall (A). Keeping machining parameters (E, T_{on}) and wall geometrical

parameters (A, L) invariably constant, the deflection at the free end is directly proportional to the ratio of α and K .

The curvature of the deflected wall resembles the deflection of a cantilever beam under point load at the free end of a beam as shown in Fig. 10a. Figure 10b shows the thin wall subjected to significant deflection at the free end. The beam deflection is maximum at the free end, and it decreases towards the fixed end.

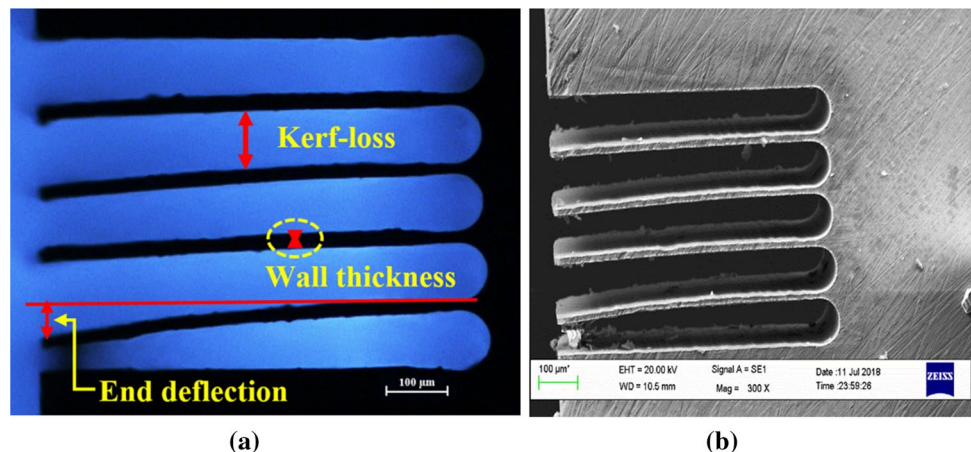
3.3 Determining the efficacy of the process

In order to establish the efficacy of the process, multi-slit thin-wall micromachining operation is conducted wherein a constant wire displacement of 92 μm is made at each pass. The value 92 μm , which is not significantly different from the minimum value of 90 μm , is chosen to determine whether the constant wall thickness is achievable and to observe the degree of wall-end deflection. The machined wall thickness obtained in this case is approximately 12–15 μm . It can be clearly seen in Fig. 11 that the wall having a thickness of about 12–15 μm is perfectly stable and free from any significant deflection at the free end. It shows that the micro-WEDM process with RC-based power generator is capable of fabricating ultra-thin wall of Ti–6Al–4V without being much affected by the thermal stresses generated in the wall.

3.4 Comparative assessment of wall deflection for different workpiece materials

Experiments are performed on three different workpiece materials namely Ti–6Al–4V, mild steel, and SS-304 to show the comparative analysis of wall-end deflection and volumetric material removal rate (MRR_v). The experimental conditions for all the three materials are selected to be constant as discharge energy of 0.72 μJ , wire feed rate of 6 $\mu\text{m/s}$, and wire speed of 10%, respectively. The wire displacement

Fig. 11 Multi-slit thin-wall micromachining at constant wire displacement of 92 μm **a** optical microscopic image, **b** SEM image (at discharge energy: 0.72 μJ and wire feed rate: 6 $\mu\text{m/s}$)



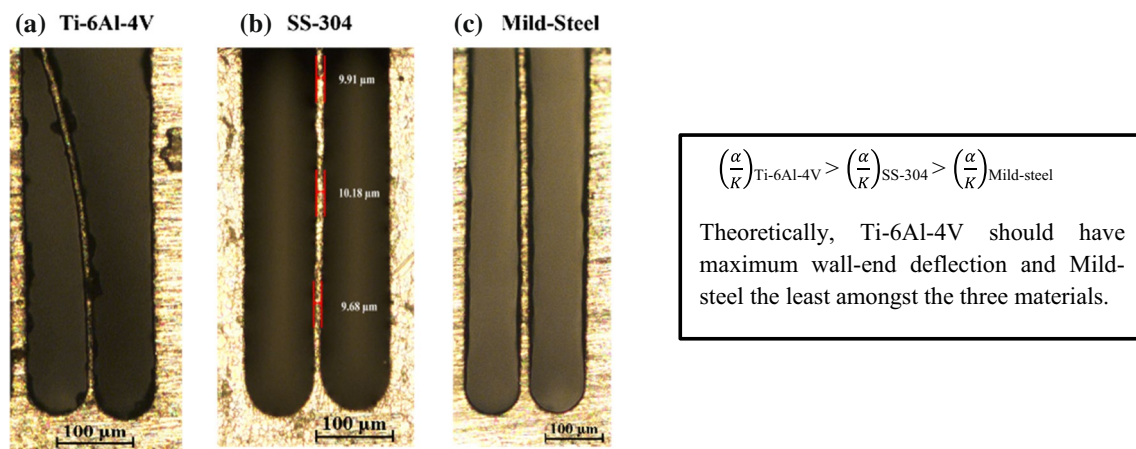


Fig. 12 Optical microscopic image of thin wall machined **a** on Ti-6Al-4V, **b** on the SS-304, **c** on mild steel workpiece

approach is adopted for the thin-wall machining on the above-mentioned materials.

Figure 12 illustrates the optical microscopic images of the thin-wall machining performed on the aforementioned three workpiece materials. It has been established that at constant wire displacement of 90 μm , the wall thickness, its end deflection, and volumetric material removal rate (MRR_v) are not equal. It can be elucidated by the fact that the thermo-physical properties of workpiece material such as the coefficient of linear expansion and thermal conductivity are the decisive factors in determining the output responses. Under identical conditions of input parameters and wall length, the end deflection is directly proportional to the ratio of coefficient of linear expansion to thermal conductivity. This ratio is highest for Ti-6Al-4V followed by SS-304 and mild steel. Therefore, Ti-6Al-4V experiences the highest end deflection and mild steel the lowest. The minimum average wall thickness obtained at the above-mentioned conditions for all three materials are slightly different. The average wall thickness is minimum for Ti-6Al-4V and highest for mild steel due to which the end deflection has a significant difference. The end deflection of the thin wall machined on Ti-6Al-4V is measured to be 69 μm , whereas for SS-304 and mild steel it is 9 μm and 7.5 μm , respectively. The end deflection for SS-304 and mild steel is significantly low as both the materials have a very high thermal conductivity as compared to Ti-6Al-4V. Also, the difference in the thermal conductivities of mild steel and SS-304 is too small, which indicates the similar deflection in both cases. The high thermal conductivity of material leads to better diffusion of heat from the wall to the surrounding dielectric fluid and diminishes the deflection of the wall due to thermal stresses. However, the effective diffusion of heat due to good thermal conductivity results in the lower volume of material removal per pulse as the conduction of heat reduces the amount of available thermal energy for material removal.

Table 2 MRR_v , wall-end deflection, and average wall thickness for three workpiece materials

Workpiece material	Ti-6Al-4V	SS-304	Mild steel
MRR_v ($10^3 \mu\text{m}^3/\text{s}$)	59.29	48.94	14.26
Wall-end deflection (μm)	69	9	7.5
Average wall thickness (μm)	8.47	9.91	13.11

This fact is verified by calculating the MRR_v for the three materials. Ti-6Al-4V due to its poor thermal conductivity as compared to the other two materials results in the highest material removal rate, whereas mild steel results in the lowest volumetric material removal rate ($\mu\text{m}^3/\text{s}$) among the three materials. MRR_v , wall-end deflection, and average wall thickness for all the three materials are shown in Table 2. The wall generation rate can be correlated with the MRR_v by just dividing it with the average kerf-loss and the thickness of the workpiece. However, if the thickness of the workpieces is slightly different, MRR_v is the only appropriate means to compare the machining rate realized with the three materials.

4 Conclusions

The present work demonstrated the aspect of thin-wall micromachining using micro-WEDM process. Observations from the rigorous experimental study suggest that a wall with an average thickness of 15 μm can be machined using this method without any appreciable deflection due to thermal stresses. However, when the discharge energy was reduced to 0.72 μJ , a minimum average wall thickness of 8.47 μm is fabricated, but it was subjected to an end deflection. A mathematical expression for the end deflection of

the wall was derived, which suggests its dependency on wall geometric parameters, discharge parameters, and workpiece thermophysical properties in different proportions. It has also been observed that Ti–6Al–4V offered maximum wall generation rate (followed by SS-304 and least in mild steel), but also experienced maximum wall-end deflection prominently due to the difference in their thermal properties. This work can be extended to determine theoretically and numerically the minimum possible wall thickness in terms of thermophysical properties of workpiece material and different process parameters.

References

- Wang F, Cheng X, Zheng GM, Yang XH, Guo QJ, Sun QL (2019) Study of micromilling parameters and processes for thin wall fabrications. *Precis Eng* 56:246–254. <https://doi.org/10.1016/j.precisioneng.2018.12.005>
- O'Mahony C, Hill M, Hughes PJ, Lane WA (2002) Titanium as a micromechanical material. *J Micromech Microeng* 12:438–443
- Ohshita Y, Kojima T, Suzuki R, Kinoshita K, Kawatsu T, Nakamura K, Ogura A (2017) High quality and thin silicon wafer for next generation solar cells. In: IEEE 44th photovoltaic specialist conference (PVSC). IEEE, Washington, pp 2588–2592
- Sakamoto S, Hayashi K, Kondo Y, Yamaguchi K, Fujita T, Yakou T (2016) Fundamental micro-grooving characteristics of hard and brittle materials with a fine wire tool. *Adv Mater Res* 1136:299–304. <https://doi.org/10.4028/www.scientific.net/AMR.1136.299>
- Wu H (2016) Wire sawing technology: a state-of-the-art review. *Precis Eng* 43:1–9. <https://doi.org/10.1016/j.precisioneng.2015.08.008>
- Liu J, Li L (2006) Direct fabrication of thin-wall parts by laser cladding. *J Manuf Process*. [https://doi.org/10.1016/S1526-6125\(06\)70096-2](https://doi.org/10.1016/S1526-6125(06)70096-2)
- Joshi K, Ananya A, Bhandarkar U, Joshi SS (2017) Ultra thin silicon wafer slicing using micro-WEDM for solar cell application. *Mater Des* 124:158–170. <https://doi.org/10.1016/j.matdes.2017.03.059>
- Rakwal D, Bamberg E (2009) Slicing, cleaning and kerf analysis of germanium wafers machined by wire electrical discharge machining. *J Mater Process Technol* 209:3740–3751. <https://doi.org/10.1016/j.jmatprotec.2008.08.027>
- Luo YF, Chen CG, Tong ZF (1992) Investigation of silicon wafering by wire EDM. *J Mater Sci* 27:5805–5810
- Takino H, Ichinohe T, Tanimoto K, Yamaguchi S, Nomura K, Kunieda M (2004) Cutting of polished single-crystal silicon by wire electrical discharge machining. *Precis Eng* 28:314–319. <https://doi.org/10.1016/j.precisioneng.2003.12.002>
- Takino H, Ichinohe T, Tanimoto K, Yamaguchi S, Nomura K, Kunieda M (2005) High-quality cutting of polished single-crystal silicon by wire electrical discharge machining. *Precis Eng* 29:423–430. <https://doi.org/10.1016/j.precisioneng.2004.12.004>
- Joshi K, Bhandarkar U, Samajdar I, Joshi Suhas S (2018) Micro-structural characterization of thermal damage on silicon wafers sliced using wire-EDM. *J Manuf Sci Eng* 140:9. <https://doi.org/10.1115/1.4039647>
- Dongre G, Zaware S, Dabade U, Joshi SS (2015) Multi-objective optimization for silicon wafer slicing using micro-WEDM process. *Mater Sci Semicond Process* 39:793–806. <https://doi.org/10.1016/j.mssp.2015.06.050>
- Wu X, Li S (2018) Experimental investigations of a hybrid machining combining wire electrical discharge machining (WEDM) and fixed abrasive wire saw. *Int J Adv Manuf Technol* 95:2613–2623. <https://doi.org/10.1007/s00170-017-1357-z>
- Miller SF, Kao CC, Shih AJ, Qu J (2005) Investigation of wire electrical discharge machining of thin cross-sections and compliant mechanisms. *Int J Mach Tools Manuf* 45:1717–1725. <https://doi.org/10.1016/j.ijmactools.2005.03.003>
- Zhang Y, Zhang Z, Huang H, Huang Y, Zhang G (2018) Study on thermal deformation behavior and microstructural characteristics of wire electrical discharge machining thin-walled components. *J Manuf Process* 31:9–19. <https://doi.org/10.1016/j.jmapro.2017.10.024>
- Zhang Y, Guo S, Zhang Z, Huang H, Li W, Zhang G, Huang Y (2019) Simulation and experimental investigations of complex thermal deformation behavior of wire electrical discharge machining of the thin-walled component of Inconel 718. *J Mater Process Technol* 270:306–322. <https://doi.org/10.1016/j.jmatprotec.2019.02.020>
- Mohd S, Omar H, Abd I (2012) High sensitive piezoresistive cantilever MEMS based sensor by introducing stress concentration region (SCR). In: Finite element analysis: new trends. <https://doi.org/10.5772/48426>
- Acheli A, Serhane R (2014) Mechanical behavior simulation of MEMS-based cantilever beam using COMSOL multiphysics. In: 4th international congress in advanced applied physics and material science (APMAS 2014) AIP, 2015, no 020005, pp 1–8. <https://doi.org/10.1063/1.4914196>
- Syam WP, Al-Shehri HA, Al-Ahmari AM, Al-Wazzan KA, Mannan MA (2012) Preliminary fabrication of thin-wall structure of Ti–6Al–4V for dental restoration by electron beam melting. *Rapid Prototyp J* 18(3):230–240. <https://doi.org/10.1108/1355254121218180>
- Najmi M, Abd Wahid MH, Wahab Y, Anuar AFM, Fazmir H, Johari S, Mazalan M (2014) MEMS parallel plate beam actuator: correlation study of pull-in voltage and dielectric layer beyond 1 μm displacement. In: Conference proceedings on paper – sensors and applications, pp 1–4
- Bergers LJJ, Hoefnagels JPM, Geers MGD (2011) MEMS and nanotechnology. In: Volume 4: proceedings of the 2011 annual conference on experimental and applied mechanics
- Karthikeyan G, Ramkumar J, Dhamodaran S, Aravindan S (2010) Micro electric discharge milling process performance: an experimental investigation. *Int J Mach Tools Manuf* 50:718–727. <https://doi.org/10.1016/j.ijmactools.2010.04.007>
- Singh M, Ramkumar J, Rao RV, Balic J (2019) Experimental investigation and multi-objective optimization of micro-wire electrical discharge machining of a titanium alloy using Jaya algorithm. *Adv Prod Eng Manag* 14(2):251–263. <https://doi.org/10.14743/apem2019.2.326>
- Yeo SH, Kurnia W, Tan PC (2007) Electro-thermal modelling of anode and cathode in micro-EDM. *J Phys D Appl Phys* 40(8):2513–2521. <https://doi.org/10.1088/0022-3727/40/8/015>
- Jain VK (2007) Advanced machining processes. Allied Publishers Private Limited, New Delhi
- Masuzawa T, Tonshof HK (1997) Three-dimensional micromachining by machine tools. *Ann CIRP* 46(2):621–628. [https://doi.org/10.1016/S0007-8506\(07\)60882-8](https://doi.org/10.1016/S0007-8506(07)60882-8)

Publisher's Note Springer Nature remains neutral with regard to jurisdictional claims in published maps and institutional affiliations.